Intrinsic and precipitate-induced quantum corrections to conductivity in $La_{2/3}Sr_{1/3}MnO_3$ thin films

Yuze Gao,[1,2] Guixin Cao,[3] Jincang Zhang,[2] and Hanns-Ulrich Habermeier[1,2,*]

[1]*Max Planck Institute for Solid State Research, Heisenbergstrasse 1, D-70569 Stuttgart, Germany*

[2]*Department of Physics, Shanghai University, Shanghai 200444, People's Republic of China*

[3]*Department of Materials Science and Engineering, University of Tennessee, Knoxville, Tennessee 37996, USA*

(Received 15 November 2011; published 14 May 2012)

The low-temperature magnetotransport properties of manganite thin films are characterized by the occurrence of resistivity minima, ρ_{min}, below 30 K whose origin and especially role of disorder has not yet been explored in detail. In order to contribute to the clarification of the physical mechanism giving rise to the resistivity minimum in these systems, an appropriate concentration (3%, 6%, and 20%) of nanoscaled nonmagnetic ZrO_2 particles are introduced as a secondary phase into $La_{2/3}Sr_{1/3}MnO_3$ thin films. As the volume density of ZrO_2 precipitates increases, the films show a more pronounced resistivity upturn for $T < T_{min}$. The measured temperature and magnetic field dependence of the resistivity of our samples is in good agreement with a combination of the theory of three-dimensional weak localization and electron-electron interactions. We show that within this frame the observed features of the scattering-related resistivity minimum at low temperature in correlated electron systems can be explained, including its spin dependence, its scattering parameters, and its variation with increasing nonmagnetic disorder.

DOI: 10.1103/PhysRevB.85.195128 PACS number(s): 72.15.Rn, 75.20.Hr, 75.47.Lx, 77.22.Ej

I. INTRODUCTION

The transport properties of strongly correlated electron systems depend sensitively on disorder, and its role in determining the physical properties of these systems, especially the low-temperature magnetoresistance, is not yet fully understood.[1–6] In the past decade, several papers have been published claiming the presence of quantum interference effects in the low-temperature region of the magnetotransport properties which give rise to resistivity minim, ρ_{min}, below ~40 K.[7–10] These resistivity minima—appearing to be similar to those of Kondo systems—were observed in manganite bulk ceramics,[11] polycrystalline as well as high-quality epitaxially grown films, and single crystals.[12–15] Extensive experimental and theoretical work has been performed, and several mechanisms have been discussed to interpret these resistivity minima. Among them are mechanisms based on spin-polarized tunneling via grain boundaries,[16] Kondo-like effects (magnetic and charge type),[17–19] and quantum interference effects (QIEs) arising from electron-electron interactions and weak localization,[1,12] just to name a few. However, a clear picture has not yet emerged and is still under discussion,[9,20] impeding our understanding of the physics of correlated electron systems. Reviewing these existing explanations, the question of whether or not the scattering-related minimum at low temperature is a spin-dependent effect emerged as a key issue in its understanding. In previous experiments Maritato *et al.*[21] used epitaxially grown single-phase $La_{0.7}Sr_{0.3}MnO_3$ (LSMO) films and found an upturn of resistivity below 60 K. This effect was studied as a function of film thickness and magnetic field and a thickness-dependent crossover from 3D to 2D behavior was observed. They interpreted their results as an interplay of electron-electron interaction (EEI) and localization effects, however, leaving all defect-related contributions to the magnetoresistance as an open question. Chen *et al.*[11] analyzed the correlation of low-temperature resistivity minima with magnetic properties for optimally doped $La_{0.67}Ca_{0.33}MnO_3$ bulk samples and related their results to e^--e^- interaction and spin-disorder scattering. Jia *et al.*[4] investigated effects of ferroelectric poling-induced strain on the quantum corrections to low-temperature resistivity of sputtered $La_{0.7}Ca_{0.15}Sr_{0.15}MnO_3$ films and interpreted the resistivity upturn in terms of QIE effects originating from inelastic scattering and e^--e^- interactions enhanced by disorder.

In order to contribute to the clarification of the physical mechanism of the resistivity minimum in magnetically ordered systems and to check the role of spin-dependent effects associated with ρ_{min}, some dedicated experiments applying a systematic variation of one material-related parameter will be necessary. We have chosen thin films with a constant thickness (54 nm) of the ferromagnet $La_{2/3}Sr_{1/3}MnO_3$ and introduced nanoscaled nonmagnetic ZrO_2 particles with an appropriate concentration (0, 3%, 6%, and 20%) as a secondary phase. To prepare such films pulsed laser deposition (PLD) was applied as a preparation technique. The magnetic field and temperature dependence of the transport properties were systematically studied. LSMO was chosen because of its characteristic ferromagnetic metallic phase with a temperature-induced metal-insulator transition and half-metallic conductivity.[22–24] By controlling the concentration of nonmagnetic ZrO_2, one can investigate the disorder effect of nonmagnetic particles without changing the spin condition of the matrix. By means of a detailed analysis of the resistivity as a function of magnetic field, temperature, and density of nonmagnetic ZrO_2 particles, the origin of resistivity minima is found to be in good agreement with a combination of the theory of 3D weak localization and electron-electron interaction in the metallic LSMO system with nonmagnetic disorder. The relevance of the quantum nature of these effects is justified by the closeness of the mean-free path l (typically <5.7 nm) to the Fermi wavelength $\lambda_F = 2\pi/k_F$ (~0.35 nm) of the electrons where the simple kinetic theory of conductivity is expected to break down. Nonmagnetic ZrO_2 particles in the metallic LSMO thin films modify the diffusion constant and increase the contribution of weak localization at low

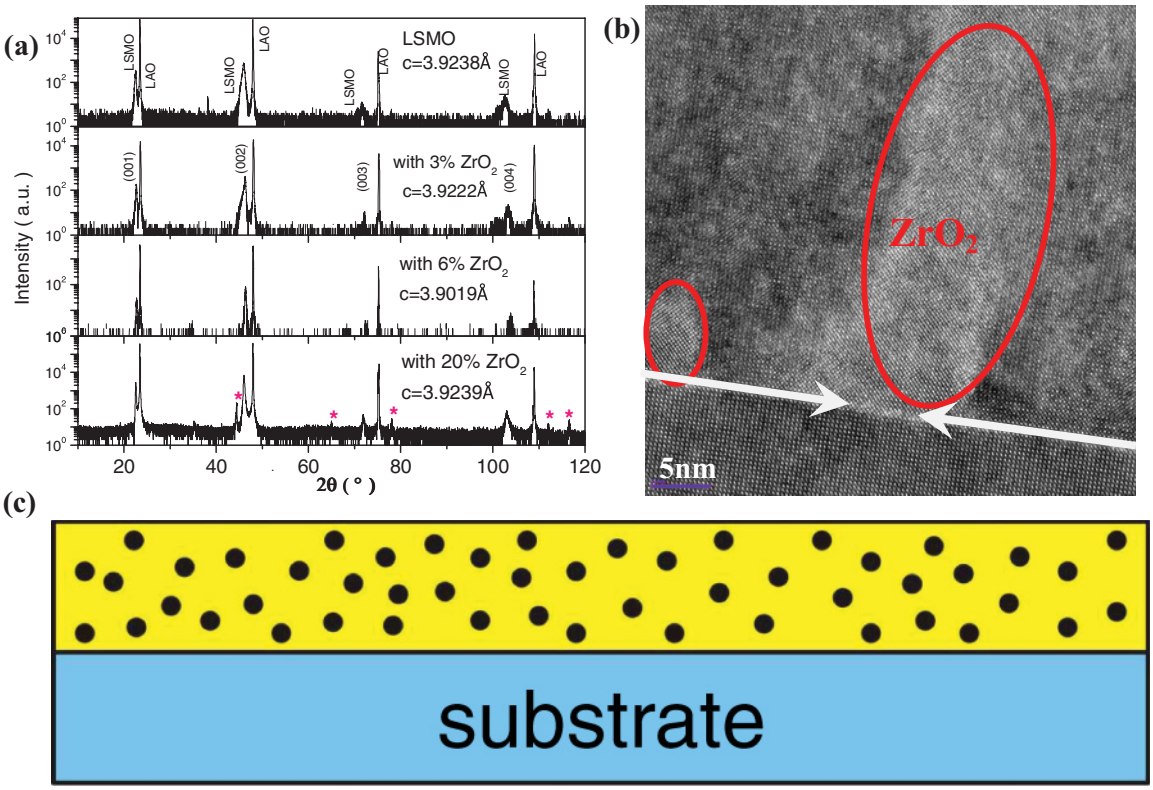

FIG. 1. (Color online) (a) X-ray diffraction pattern for the (h00) reflections of LSMO, LAO, and ZrO_2 nanoclusters. The red asterisks mark the ZrO_2 reflections. (b) High-resolution TEM image of the cross-sectional specimen of LSMO with 6% ZrO_2 cluster thin film on LAO in [001] zone. The interface is marked with arrows. (c) Schematic sketch of the introduced nonmagnetic ZrO_2 nanoparticles in the LSMO matrix. The bottom part presents LAO substrate.

temperatures. Our results provide experimental confirmation of the weak localization and electron-electron interaction effect in ferromagnetic oxide thin films with nonmagnetic disorder.

II. EXPERIMENT DETAILS

Manganite targets with the nominal composition $La_{2/3}Sr_{1/3}MnO_3$ were prepared using standard solid state reaction methods. Appropriate ratios of La_2O_3, $SrCO_3$, and MnO_2 powder were intimately mixed and ground using a semiplanetary ball mill. The powder was sintered twice at 1300 °C for 12 h, with intermediate grindings. Pellets with a diameter of 12 mm were uniaxially cold pressed and sintered at 1300 °C for 12 h in air to be used as high-density targets. Targets with different ZrO_2 content were prepared using intimately mixed and ground stoichiometric amounts of LSMO and ZrO_2 according to $(1-x)La_{2/3}Sr_{1/3}MnO_3+xZrO_2$, with $x = 0.03, 0.06, 0.2$. Pellets with a diameter of 12 mm were uniaxially cold pressed and sintered at 800 °C for 12 h in air, which can prevent Zr^{4+} from entering the manganite matrix.

Thin films of $(1-x)$LSMO$+x$$ZrO_2$ were grown on 5 × 5 × 0.5 mm^3 single-crystal substrates of (100)-oriented $LaAlO_3$ (LAO) using the standard PLD techniques applying the following parameters: KrF excimer laser ($\lambda = 248$ nm), repetition rate 2 Hz, photon fluency 1.6 J/cm^2, deposition temperature 770 °C, and oxygen pressure 0.4 mbar. After deposition, the films were annealed 30 minutes at 630 °C in 4.7 × 10^2 mbar oxygen pressure to ensure full oxidation followed by a cooling process down to room temperature in 1 atm oxygen. In each deposition run four substrates have been used and the films were subsequently taken for the measurements. The thickness of the thin films was determined by pulse counting during the PLD process and measured to be 54 nm using a profilometer as well as during the preparation steps for high-resolution transmission electron microscopy (HR-TEM). X-ray diffraction (XRD) was performed on all films using a Bruker AXS-D8 x-ray diffractometer with $Cu_{K\alpha}$ radiation. The electrical resistance was measured using four stripe contacts on unpatterned samples with evaporated chromium/gold (20 nm/200 nm) pads as current and voltage probes. Resistivity measurements were carried out using a PPMS-9 (Quantum Design) system. The magnetization (M) has been measured in a SQUID magnetometer (Quantum Design). Using different samples from each run and measuring the resistance with different heating/cooling rates, all the experimental results are nicely reproducible. Aging effects could not be observed.

III. RESULTS AND DISCUSSION

A. Structural and magnetic characterization

In Fig. 1(a) the XRD patterns for samples deposited from targets with 0, 3%, 6%, and 20% ZrO_2 additions are depicted. The films with a nominal ZrO_2 volume fraction of 6% and less show in addition to the (00l) LAO substrate peaks only (00l)

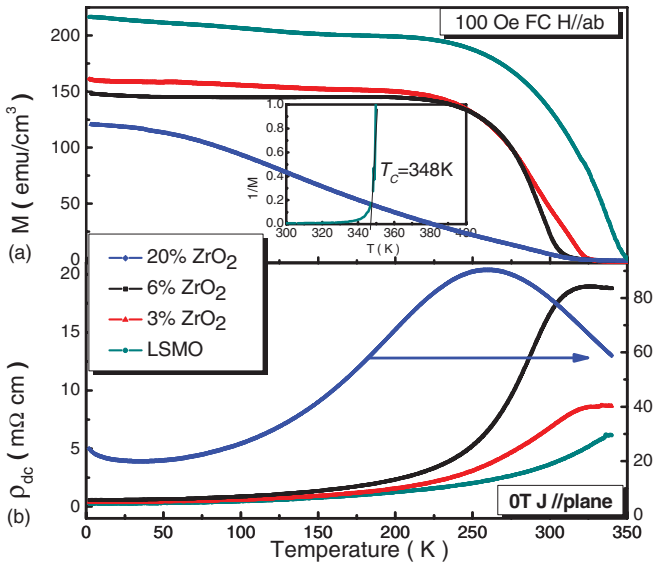

FIG. 2. (Color online) Temperature dependence of (a) the magnetization and (b) the resistivity of the single-crystal LSMO thin films with 0, 3%, 6%, and 20% ZrO_2. Inset (a): The Curie-Weiss fit for the determination of T_C for pure LSMO thin film.

peaks from LSMO. The out-of-plane lattice parameter was determined to be $c = 3.924$ Å for LSMO, with a slight decrease with increasing density of ZrO_2 precipitates ($c = 3.902$ Å for the 6% ZrO_2 sample). This indicates a compressive strain of the films ($a_{sub} = 3.79$ Å, $a_{LSMO} = 3.86$ Å). In samples with 20% ZrO_2, the c-axis lattice parameter relaxes to the original value and additional diffraction peaks appear associated with ZrO_2; they can be regarded as two-phase materials. The presence of ZrO_2 precipitates is confirmed by HR-TEM investigations. Figure 1(b) shows the cross-sectional HR-TEM image of a LSMO film with 6% ZrO_2 added. It clearly illustrates the cube-on-cube epitaxial growth relation of the LSMO matrix in the interfacial region close to the substrate and the appearance of nanoscaled ZrO_2 clusters. It can be seen that the interface in general is perfectly coherent and no notable misfit dislocations were detected. It is evident that the film has a uniform LSMO structure; additional nanoscaled ZrO_2 clusters are indicated by the red circles in Fig. 1(b). Figure 1(c) illustrates the statistical distribution of the ZrO_2 precipitates schematically. The temperature dependence of the magnetization M and the resistivity ρ_{dc} of the single-crystal thin films are presented in Fig. 2. The Curie temperature $T_C = 348$ K of pure LSMO film was determined by extrapolating the measured M-T data according to the Curie-Weiss law at $1/M = 0$ [as shown in the inset of Fig. 2(b)], indicating the high quality of our thin films. With increasing density of ZrO_2 nanoparticles, T_C decreases and the transition width widens. Accordingly, as the temperature is decreased in the paramagnetic phase, the resistivity increases and reaches a maximum around T_C, which can be attributed to a small polaron hopping mechanism.[25] In the ferromagnetic region ($T < T_C$), the samples show a metallic behavior at low temperatures. However, the resistivity does not show a residual resistance behavior for $T \to 0$, but reaches a doping-dependent minimum around 10 K to 30 K followed by a slow increase as the temperature is lowered down to 2 K. Enhancing the density of ZrO_2 nanoparticles affects the ferromagnetic ordering as well as the transport properties at low temperatures. In order to reveal the origin of the resistivity minimum and clarify the influence of nonmagnetic ZrO_2 nanoparticles in the system, the electrical transport properties were studied in detail.

B. Electrical transport measurements

The temperature dependence of the resistivity of the ZrO_2-doped thin films is shown in an expanded scale in Fig. 3 for temperatures below 40 K. The resistivity of films without ZrO_2 particles behaves like a typical metal at low temperature, however, with a faint indication of a resistance anomaly. The ZrO_2-doped thin films show a distinct resistivity upturn for $T < T_{min}$. The pure metallic behavior is expected in films where the mean-free path l of the carriers is much larger than the Fermi wavelength λ_F. In that case, the low-temperature transport properties should be consistent with the semiclassical Boltzmann approach. However, as the density of nonmagnetic ZrO_2 nanoparticles increases, a higher resistivity is measured arising from the increase of the number of ZrO_2 nanoprecipitates and thus yielding a shorter mean-free path. In the following we consider several mechanisms which can be accounted for the resistivity upturn below 30 K: (a) Kondo-like mechanisms that are arising from the exchange interaction of conduction electrons with localized spin impurities, (b) weak localization[26] as a contribution due to quantum interference between two waves propagating by multiple scatters along the same path but in opposite directions, and (c) electron-electron interaction as the diffraction of one electron wave by the oscillation in the electrostatic potential generated by other electrons.

A disentanglement of the contributions can be accomplished if we make use of the effect that a strong magnetic field suppresses the contribution of weak localization.[12] Figure 4 represents the data $\Delta\rho(T) = \rho(T) - \rho_{min}$ for the different applied magnetic fields ($0\ \mathrm{T} \leqslant H \leqslant 9\ \mathrm{T}$) indicating the resistivity upturn. This approach ensures that conventional magnetoresistance effects (see Fig. 3) do not enter our analysis of the data for the resistance anomaly. We separate the data into two parts, a field-dependent part (part A) and a field-independent part (part B). To separate the field-dependent part, we used the following approach: First, we determine (for each sample) the resistivity minimum $\rho_{H\,min}$ for the different magnetic fields using the minimum value of ρ of the raw data and calculate the corresponding values for the resistivity upturn according to $\Delta\rho_H(T) = \rho_H(T) - \rho_{H\,min}$. It turns out that the values for $\rho_{H\,min}$ do not depend on the temperature. These data are plotted in Fig. 4 as dotted lines. With increasing magnetic field the contribution $[\Delta\rho_H(T)]$ decreases and our conjecture—which is proven experimentally by plotting $\Delta\rho_H - \Delta\rho_{9T}$ vs T for, e.g., $T = 2$ K and 4.2 K—is that at 9 T this contribution vanishes. This result is qualitatively consistent with the data of Chen *et al.* revealed from measurements of polycrystalline $La_{2/3}Ca_{1/3}MnO_3$ samples.[11] The physics behind this empirical finding is the vanishing of effects due to weak localization in strong magnetic fields as already stated by Ziese.[12] Consequently, the field-dependent part of the resistivity upturn is $\Delta\rho_A(T) = \Delta\rho_{0T}(T) - \Delta\rho_{9T}(T)$. For pure LSMO, $\Delta\rho_A \approx 0$, this nicely coincides with our explanation because there is no impurity (ZrO_2) in the thin film, so no

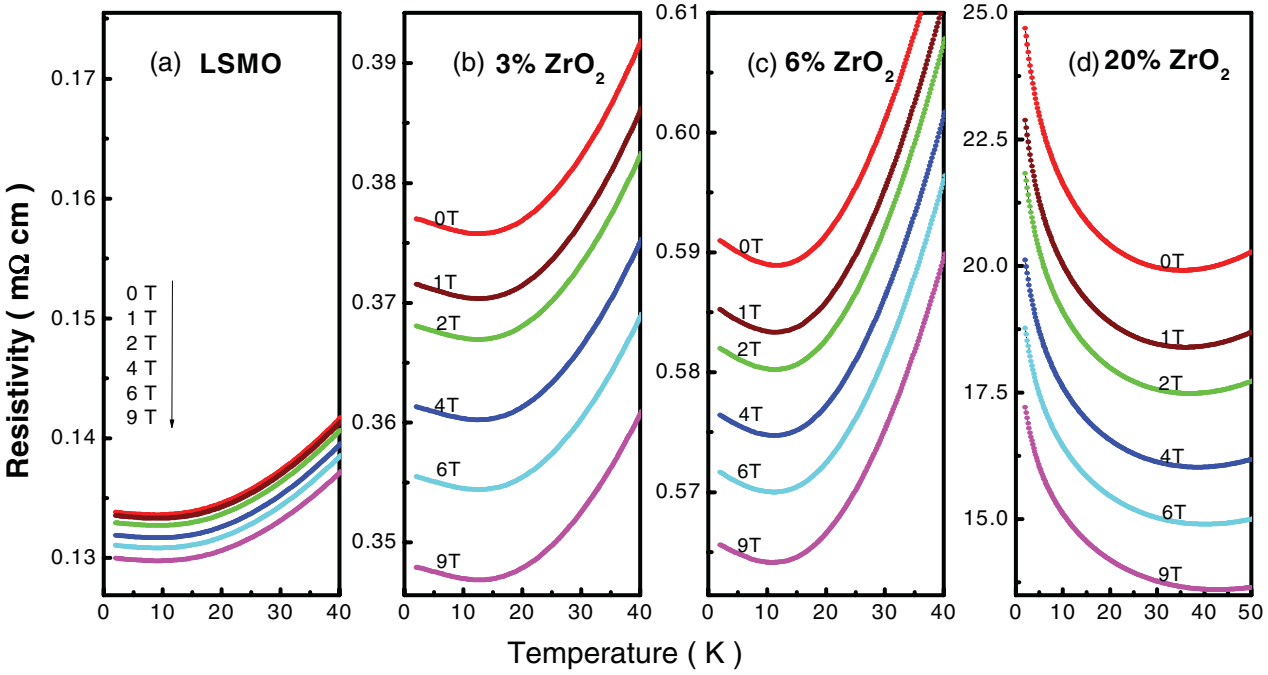

FIG. 3. (Color online) Temperature dependence of resistivity measured with various magnetic fields applied parallel to the thin film plane for 54 nm thick LSMO with 0, 3%, 6%, and 20% ZrO_2, respectively. To compare the data of 0, 3%, 6% samples, the same scale in the y axis was used in the figures, while for the 20% sample, the scale was enlarged.

contribution to weak localization, consequently no suppressed upturn region, and part A collapses.

Part B represents the part which is not sensitive to the field $\Delta\rho_B = \rho_{9T} - \rho_{9T\,\mathrm{min}}$. From this figure we can obviously observe that for pure LSMO the contribution of the field-dependent part is nearly zero. With increasing density of ZrO_2 nanoparticles, both contributions (the magnetic field dependent as well the independent part) increase, indicating a substantial contribution due to the presence of nonmagnetic ZrO_2 nanoparticles.

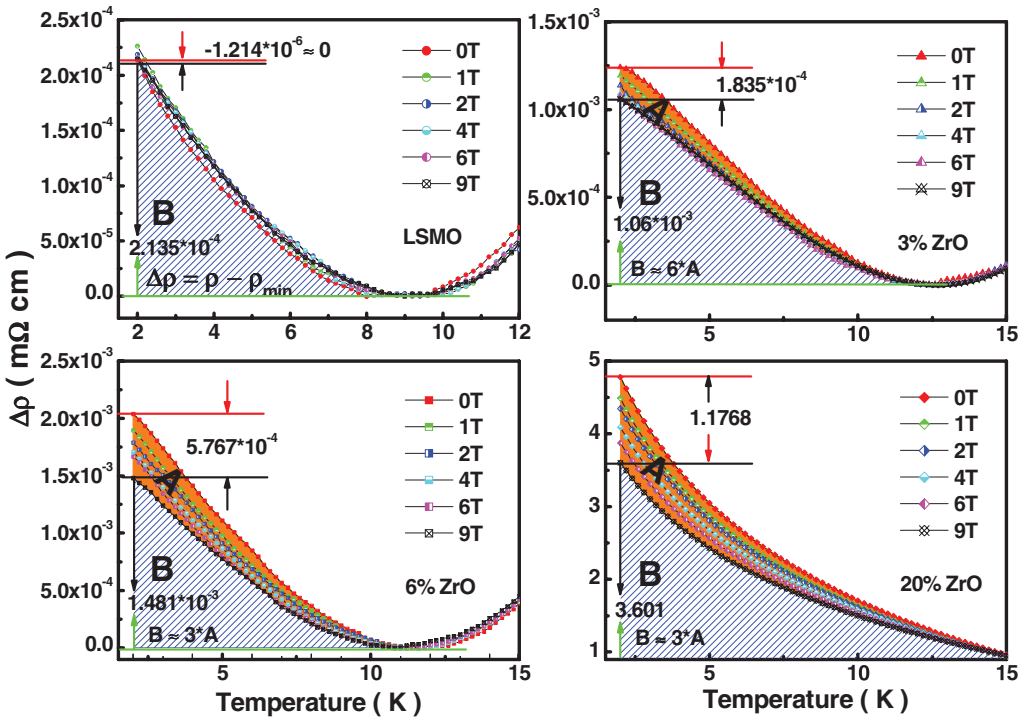

FIG. 4. (Color online) $\Delta\rho = \rho - \rho_{\mathrm{min}}$ as a function of temperature for LSMO samples with 0, 3%, 6%, and 20% ZrO_2. Part A (brown) represents the magnetic field dependent $\Delta\rho_A = \Delta\rho_{0T} - \Delta\rho_{9T}$; part B (blue dashed lines) is not sensitive to the field $\Delta\rho_B = \rho_{9T} - \rho_{9T\,\mathrm{min}}$.

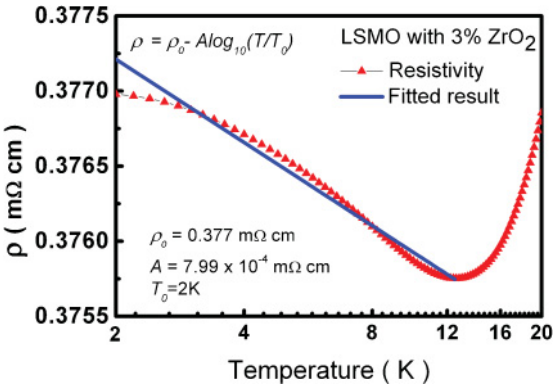

FIG. 5. (Color online) Temperature dependence of the resistivity of the single-crystal LSMO thin films with 3% ZrO_2 at low temperature and the attempt to fit the data according to the Kondo effect with $\rho \propto \log_{10} T$.

1. Kondo-like mechanisms

At first, we consider magnetic as well as charge based Kondo scattering as the dominant mechanism yielding the resistance upturn. The magnetic Kondo scattering would give rise to a $\rho \propto \log_{10} T$ behavior. In Fig. 5 the experimental resistivity in zero magnetic field is depicted together with a fit of the $\rho \propto \log_{10}(T/T_0)$ curve for a sample with 3% ZrO_2 at low temperatures. It is obvious that the $\log_{10}$-T dependence is not compatible with our results for the resistivity. An additional argument to rule out the Kondo effect comes from the magnetic field dependence of resistivity associated with the Kondo effect. Comparing the energy scale set by the Kondo temperature $k_B T_K$ and that of a magnetic field $\mu_B B$, resistivity contributions are expected to decrease in an applied magnetic field and collapse at an upper limit at $B = (k_B/\mu_B)T_K$.[17,27] Taking the temperature of the resistivity minimum as the Kondo temperature (e.g., 9 K for the undoped film) this field would be ~13 T. The data shown in Fig. 3 clearly demonstrate the existence of an upturn of ρ for $T < T_{\min}$ and no magnetic field dependence of either $T_{\min}$ or $D\rho/\rho_{\min}$; consequently the possibility of magnetic Kondo contribution to the upturn can be excluded as a relevant mechanism. However, this nearly unchanged $T_{\min}$ in a magnetic field maybe point toward the possibility of charge Kondo effect. The charge Kondo effect—proposed for the negative-U Anderson model—requires dilute impurities with two degenerate charge states and arises from quantum fluctuations.[19] This effect can be ruled out based on the following arguments: First, zirconium is not a mixed valence element and only Zr^{4+} is observed in ionic compounds, so there is no possibility to drive a negative effective U[19] and thus a charge Kondo phenomenon. Second, Zr^{4+} ions exist only in ZrO_2 nanoparticles in the films and do not enter the lattice as a dopant. The results from XRD and TEM analysis rule out this possibility.

2. 3D weak localization

Taking a Fermi wavelength of LSMO of $\lambda_F \approx 0.35$ nm,[28] the mean-free path l of the analyzed LSMO thin film ($t = 54$ nm) can be estimated from the Drude relation $\sigma = ne^2\tau/m^* = ne^2 l\lambda_F/h$, with $n \approx 10^{28}$ m^{-3}. For our LSMO thin films, the experimental value of σ is $\sigma \approx 7.7 \times 10^5$ Ω^{-1} m^{-1} at 2 K, yielding l to be $l \approx 5.7$ nm. Since the Fermi wavelength λ_F and the mean-free path are much smaller than our sample thickness of 54 nm, the three-dimensional models of weak localization and e-e interaction are applicable.

To reveal the physical mechanism for the resistivity upturn, we first discuss the contribution of weak localization (WL). The standard formula for the conductivity correction due to WL for a sample with a square cross section of width w in the 3D regime (where $w \gg \pi L_\varphi$) is [1,29,30]

$$\sigma_{\mathrm{WL}} = -\frac{e^2}{2\pi^2\hbar}\left(\frac{1}{l} - \frac{1}{L_\varphi}\right), \tag{1}$$

where l denotes a temperature-independent cutoff length on the order of the electron mean-free path and L_φ is the inelastic scattering length $L_\varphi = (D\tau_\varphi)^{1/2}$ with the diffusion constant $D = \sigma_0/[e^2 N(E_F)]$ and the inelastic lifetime τ_φ. If we take $\tau_\varphi = (a^2/D)T^{-p}$, where p is an index depending on scattering mechanism and dimensionality, we get $L_\varphi = aT^{-p/2}$.

In order to quantitatively analyze the contribution of WL to the resistivity upturn further, we argue that a magnetic field of 9 T will be enough to suppress WL[12] and the difference between the zero-field data and the 9 T data can be attributed to the weak-localization contribution $\sigma_{\mathrm{WL}} = \Delta\sigma_{9T} - \Delta\sigma_{0T}$. The fit of the low-temperature ($T < 30$ K) conductivity data $\sigma_{\mathrm{WL}} = \Delta\sigma_{9T} - \Delta\sigma_{0T}$ according to Eq. (1) is shown in Fig. 6. Here, the symbols are the experimental data and the solid lines are the fitting curves. We see clearly that an increase of the concentration of ZrO_2 precipitates causes a continuous increase of the contribution attributed to weak localization. Furthermore, we observe a tendency that, corresponding to the resistivity minimum, shifts to higher values with increasing density of nonmagnetic ZrO_2 particles. The temperature region where the data can nicely be described by Eq. (1) increases with increasing ZrO_2 particle density from nearly 10 K for 3%, 6% ZrO_2 to more than 16 K for 20% ZrO_2. This shows an enhancement of the contribution of weak localization due to ZrO_2 nanoparticles. The weak localization arises from quantum interference between electronic paths and thus modifies the diffusion constant. The fit parameters l, a, and p for samples with different ZrO_2 particle densities as displayed in Table I give further information concerning the precipitate dependence of the scattering parameters of our samples.

3. Electron-electron interaction

The analysis of the data within the frame of the WL theory shows that additional reasons for the resistivity upturn must be at work. This can be seen in the ρ-T curves of Fig. 3 at high magnetic field where the resistivity at $B = 9$ T definitely shows a pronounced upturn with decreasing temperature. Since the WL can be suppressed by a magnetic field, the resistivity upturn at 9 T originates from the EEI correction to the conductivity. Figure 7 gives the temperature dependence of conductivity in an applied field of 9 T for the low-temperature region of 2–12 K for different ZrO_2 content with 0, 3%, 6%, and 20%, respectively. It can be seen that as the density of ZrO_2 nanoprecipitates in the LSMO thin film increases, the resistivity upturn strengthens. In the following

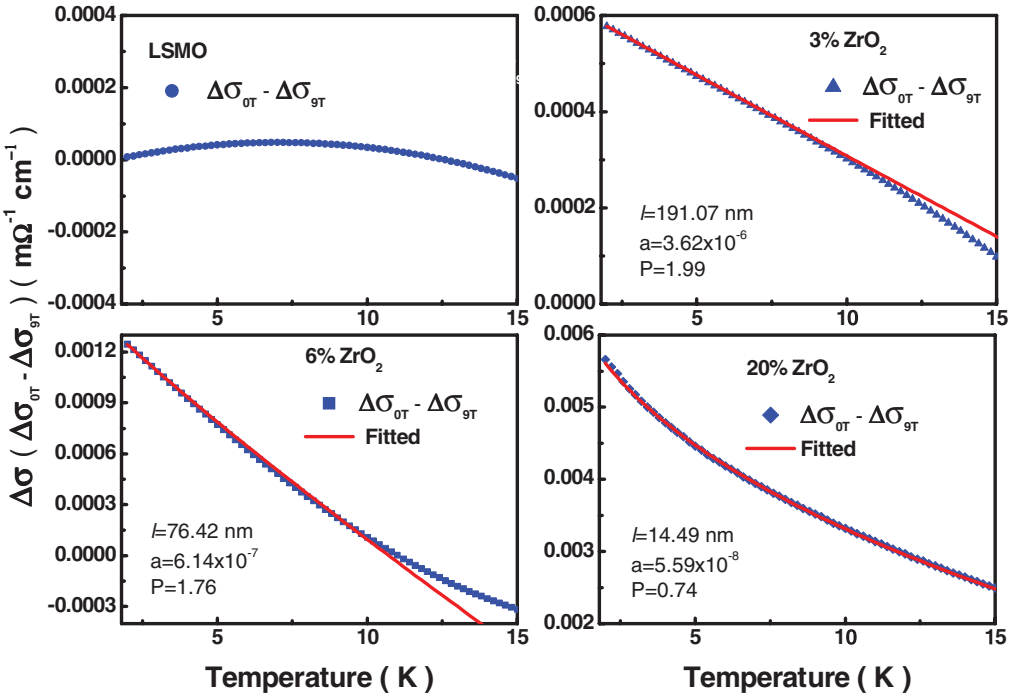

FIG. 6. (Color online) Fit of the $\Delta\sigma = \Delta\sigma_{9T} - \Delta\sigma_{0T}$ data to the weak-localization theory according to Eq. (1) for LSMO samples with 0, 3%, 6%, and 20% ZrO_2.

we apply the theory of EEI to the data for the resistivity upturn at 9 T for the samples with different density of precipitates. The contribution to the functional dependence of the conductivity due to the EEI is similar to that due to WL but with the inelastic diffusion length L_φ replaced by the thermal diffusion length $L_T = (\hbar D/kT)^{1/2}$, and a modified prefactor. In the 3D regime $\Delta\sigma_{ee}$ is given by[31]

$$\Delta\sigma_{ee} = -\left[0.46\left(\frac{4}{3} - \frac{3\tilde{F}_\sigma}{2}\right)\right]\frac{e^2}{2\pi^2\hbar}\left(\frac{1}{l} - \frac{1}{L_T}\right), \qquad (2)$$

where the interaction constant $\tilde{F}_\sigma$ is related to the screening factor F as $\tilde{F}_\sigma = (32/3F)[(1 + F/2)^{3/2} - 1 - (3F/4)]$.[1] The resulting fits according to Eq. (2) are presented in Fig. 7 (solid lines). It is found that the experimental data of pure LSMO can be excellently described by Eq. (2) for the temperature range below 6 K. With increasing concentration of ZrO_2 precipitates, the regions with a good fit increase, indicating that the region up to 10 K for 3% and 6% ZrO_2 can be nicely described by EEI effect. However, for 20% ZrO_2, the well-fitted region shrinks again. From these results, it can be concluded that the conductivity below $T_{\min}$ is sensitive to both electron-electron correlation and the degree of disorder. The reduction of the regime where Eq. (2) holds for the 20% ZrO_2 sample may be due to contributions arising from the electron-phonon interaction ($\Delta\sigma_{e-ph}$) in strongly disordered systems. The $\Delta\sigma_{e-ph}$ contribution cannot be suppressed by magnetic field and it is difficult to separate it from the $\Delta\sigma_{ee}$ contribution. The results for the samples with 0, 3%, and 6% ZrO_2 can be described well by Eq. (2) indicating that the weak disorder introduced did not affect the dominating role of EEI at the upturn region of the resistivity. For the strong disorder as in the 20% ZrO_2 sample, the enhanced electron-phonon interaction cannot be neglected compared to the EEI. To confirm this, we fitted the conductivity data for 9 T according to $\sigma_{9T} = \sigma_0 + \Delta\sigma_{ee} + \Delta\sigma_{e-ph}$ with $\Delta\sigma_{e-ph} = \beta T^{-3}$ as shown in Fig. 8. From this figure, it can be seen that the experimental data agree well for the temperature region up to 25 K which confirms the important role of both electron-phonon interaction and electron-electron interaction.

A check for the quality of the fit can be accomplished by comparing the measured values of the increase in $\Delta\sigma_{ee}$ in the

TABLE I. The fitting parameters of WL and EEI for LSMO thin film with 0, 3%, 6%, and 20% nanoscaled nonmagnetic ZrO_2 particles.

		0	3%	6%	20%
Weak localization	l (nm)	N/A	191.07	76.42	14.49
	a	N/A	3.62×10^{-6}	6.14×10^{-7}	5.59×10^{-8}
	p	N/A	1.99	1.76	0.74
e-e interaction	D (m^2/s)	5.14×10^{-6}	4.47×10^{-6}	3.79×10^{-6}	1.85×10^{-7}
	F_σ	0.15	0.55	0.76	0.87
	L (nm)	2.33	1.76	1.73	0.27

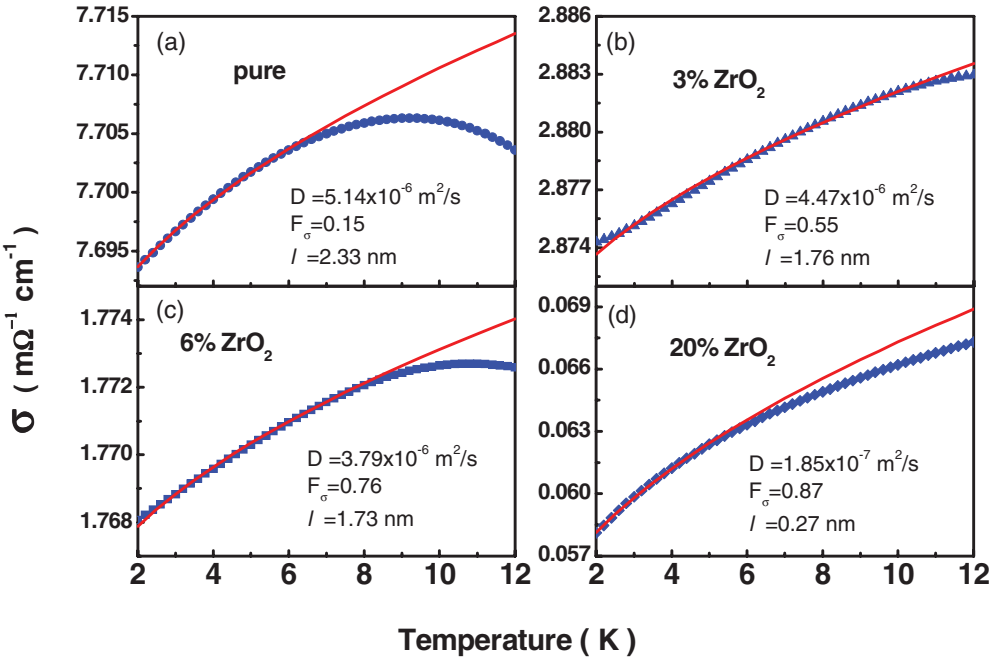

FIG. 7. (Color online) Experimental data (symbols) for the temperature dependence of conductivity at 9 T for LSMO samples with 0, 3%, 6%, and 20% ZrO_2. The solid lines are the fitting results according to Eq. (4), the expression for electron-electron interaction $\sigma_{9T} = \sigma_0 + \sigma_{ee}$.

temperature range 3 K $< T <$ 10 K with those calculated from the Altshuler-Aronov theory according to Eq. (2) using the fit parameters D, F, and l as given in Table I. For LSMO the Fermi wavelength is $k_F^{-1} = 0.056$ nm and the Thomas-Fermi screening length is $\kappa^{-1} = 1/\sqrt{8\pi\rho_0 e^2} = 0.047$ nm (where ρ_0 is the density of states per spin channel). According to the Thomas-Fermi approximation,[12,32] the screening factor F is given by $F = (\kappa/2k_F)^2 \ln[1 + (2k_F/\kappa)^2]$; therefore we obtain $F \sim 0.46$ and accordingly $\tilde{F}_\sigma = 0.44$, a value that can be compared with the fit parameter $\tilde{F}_\sigma$ in Table I. Using our fit parameter for the diffusion constant D, we can calculate L_T at 3 K and L_T at 10 K. Let us take the sample with 3% ZrO_2 as an example; the calculated conductivity difference between 10 K and 3 K due to the EEI is 689.0 $(\Omega\ \mathrm{m})^{-1}$. Together with the contribution due to weak localization [according to Eq. (1)] we get a sum of the calculated contributions to $\Delta\sigma$ between 10 K and 3 K of 712.5 $(\Omega\ \mathrm{m})^{-1}$. The magnitude of the EEI contribution to magnetoresistance exceeds the WL contribution by an order of magnitude. Experimentally the increase of conductivity for the 9 T data between 10 K and 3 K is 694.3 $(\Omega\ \mathrm{m})^{-1}$. Taking into account the measurement uncertainties and the fact that the Altshuler-Aronov theory was developed for a free electron gas and we deal with a strongly correlated electron system, this agreement is surprising. Therefore, we believe that the combined 3D theory for disordered nonmagnetic conductors is in excellent agreement with our data.

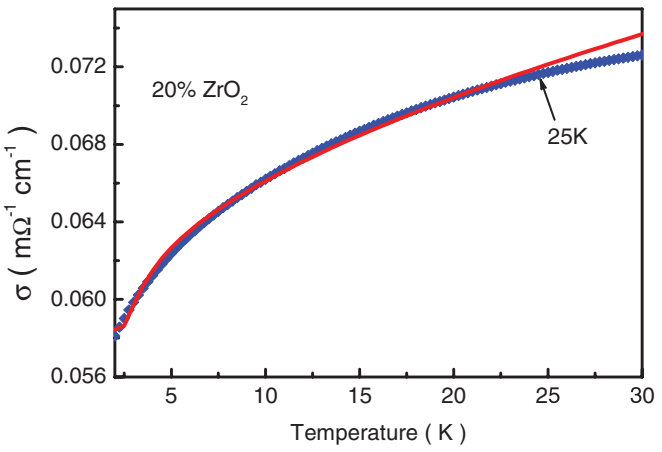

FIG. 8. (Color online) Temperature dependence of conductivity in 9 T for samples with 20% ZrO_2 and fitted to $\sigma_{9T} = \sigma_0 + \sigma_{ee} + \sigma_{e-\mathrm{ph}}$. The solid lines are the fitting results and the symbols are the corresponding experimental data.

IV. CONCLUSION

In conclusion, low-temperature transport properties of LSMO thin films with appropriate concentration (0, 3%, 6%, and 20%) nanoscaled nonmagnetic ZrO2 particles were systemically studied for applied magnetic fields ranging from 0 to 9 T. The temperature dependence of resistivity shows generally a minimum at low temperatures and a resistivity upturn that appears to be increasingly stronger with increasing ZrO_2 precipitate concentration. The temperature and magnetic field dependences of the resistivity of our samples are in good agreement with a combination of the theory of 3D weak localization and electron-electron interactions in the metallic system with nonmagnetic disorder. In particular, the presence of nonmagnetic ZrO_2 nanoparticles in the samples enhances contributions to resistivity from weak localization and electron-electron interaction. Nonmagnetic ZrO_2 particles

in the metallic LSMO thin films modify the diffusion constant and increase the weak localization at low temperature. The enhanced EEI in this 3D system is induced by the modification of the density of states due to the introduction of ZrO_2 particle. In addition, we show that our results explain the essential features of the so-called scattering-related "resistivity minimum" phenomenon at low temperature in the correlated electron systems including its spin-independent effect, its scattering parameters, and variation with increasing disorder.

ACKNOWLEDGMENTS

We are grateful to P. A. van Aken for the use of HR-TEM and to M. Kelsch for in-depth discussions of the TEM data. The valuable contributions of Y. Jing and X. Yao (target preparation), as well as B. Stuhlhofer, Y. Link, B. Lemke, and S. Schmid (various aspects of sample preparation and contacting) are acknowledged. This work is supported by the National Natural Science Foundation of China (No. 10804068 and No. 11074163) and the Science and Technology Innovation Fund of the Shanghai Education Committee (No. 12ZZ097).

*huh@fkf.mpg.de

[1] P. A. Lee and T. V. Ramakrishnan, Rev. Mod. Phys. **57**, 287 (1985).
[2] G. Singh-Bhalla, S. Selcuk, T. Dhakal, A. Biswas, and A. F. Hebard, Phys. Rev. Lett. **102**, 077205 (2009).
[3] J. Bouvier and J. Bok, J. Supercond. **15**, 651 (2002).
[4] R. R. Jia, J. C. Zhang, R. K. Zheng, D. M. Deng, H.-U. Habermeier, H. L. W. Chan, H. S. Luo, and S. X. Cao, Phys. Rev. B **82**, 104418 (2010).
[5] J. Wang, G.-Z. Liu, and H. Kleinert, Phys. Rev. B **83**, 214503 (2011).
[6] W. Pan, J. L. Reno, D. Li, and S. R. J. Brueck, Phys. Rev. Lett. **106**, 156806 (2011).
[7] X.-Y. Feng, W.-Q. Chen, J.-H. Gao, Q.-H. Wang, and F.-C. Zhang, Phys. Rev. B **81**, 235411 (2010).
[8] T. Z. Ward, Z. Gai, X. Y. Xu, H. W. Guo, L. F. Yin, and J. Shen, Phys. Rev. Lett. **106**, 157207 (2011).
[9] Y. Xu, J. Zhang, G. Cao, C. Jing, and S. Cao, Phys. Rev. B **73**, 224410 (2006).
[10] C. Barone, A. Guarino, A. Nigro, A. Romano, and S. Pagano, Phys. Rev. B **80**, 224405 (2009).
[11] Z. Chen, Y. Xu, Y. Su, S. Cao, and J. Zhang, J. Supercond. Novel Magn. **22**, 5 (2009).
[12] M. Ziese, Phys. Rev. B **68**, 132411(2003).
[13] E. Syskakis, G. Choudalakis, and C. Papastaikoudis, J. Phys.: Condens. Matter **15**, 7735 (2003).
[14] D. Kumar, J. Sankar, J. Narayan, Rajiv K. Singh, and A. K. Majumdar, Phys. Rev. B **65**, 094407 (2002).
[15] T. Okuda, T. Kimura, and Y. Tokura, Phys. Rev. B **60**, 3370 (1999).
[16] E. Rozenberg, M. Auslender, I. Felner, and G. Gorodetsky, J. Appl. Phys. **88**, 2578 (2000).
[17] T. A. Costi, Phys. Rev. Lett. **85**, 1504 (2000).
[18] J. Zhang, Y. Xu, L. Yu, S. Cao, and Y. Zhao, Physica B **403**, 1471 (2008).
[19] Y. Matsushita, H. Bluhm, T. H. Geballe, and I. R. Fisher, Phys. Rev. Lett. **94**, 157002 (2005).
[20] G.-M. Zhao, V. Smolyaninova, W. Prellier, and H. Keller, Phys. Rev. Lett. **84**, 6086 (2000).
[21] L. Maritato, C. Adamo, C. Barone, G. M. De Luca, A. Galdi, P. Orgiani, and A. Yu. Petrov, Phys. Rev. B **73**, 094456 (2006).
[22] F. Y. Bruno, J. Garcia-Barriocanal, M. Varela, N. M. Nemes, P. Thakur, J. C. Cezar, and N. B. Brookes, Phys. Rev. Lett. **106**, 147205 (2011).
[23] J.-H. Park *et al.*, Nature (London) **392**, 794 (1998).
[24] A. Chikamatsu, H. Wadati, H. Kumigashira, M. Oshima, A. Fujimori, M. Lippmaa, K. Ono, M. Kawasaki, and H. Koinuma, Phys. Rev. B **76**, 201103(R) (2007).
[25] C. Beekman, J. Zaanen, and J. Aarts, Phys. Rev. B **83**, 235128 (2011).
[26] P. Chaudhari, H.-U. Habermeier, and S. Maekawa, Phys. Rev. Lett. **55**, 430 (1985).
[27] M. Misiorny, I. Weymann, and J. Barnaš, Phys. Rev. lett. **106**, 126602 (2011).
[28] A. M. Haghiri-Gosnet, M. Koubaa, A. F. Santander-Syro, R. P. S. M. Lobo, Ph. Lecoeur, and B. Mercey, Phys. Rev. B **78**, 115118 (2008).
[29] B. Shinozaki, K. Makise, Y. Shimane, H. Nakamura, and K. Inoue, J. Phys. Soc. Jpn. **76**, 074718 (2007).
[30] A. Goldenblum, V. Bogatu, T. Stoica, Y. Goldstein, and A. Many, Phys. Rev. B **60**, 5832 (1999).
[31] R. S. Thompson, D. Li, C. M. Witte, and J. G. Lu, Nano Lett. **9**, 3991 (2009).
[32] E. Akkermans and G. Montambaux, *Mesoscopic Physics of Electrons and Photons* (Cambridge University Press, Cambridge, 2007).